Dimensionless correlations and performance maps of scroll expanders for micro-scale Organic Rankine Cycles

Luis Eric OLMEDO*, Violette MOUNIER, Luis Carlos MENDOZA, Jürg SCHIFFMANN

Laboratory for Applied Mechanical Design, École Polytechnique Fédérale de Lausanne, EPFL STI IGM LAMD (Microcity) Rue de la Maladière 71b, CP 526 CH-2002 Neuchâtel 2.
(*) corresponding author: luiseric.olmedo@epfl.ch

Keywords: Scroll expander performance, dimensionless maps, micro-ORC, distributed power systems.

In the endeavor towards distributed power systems, not seasonal-dependent micro-power generation technologies are expected to integrate the energy scenario in the years to come. In this context, the Organic Rankine Cycle (ORC) in the (1-10) KWe scale has chronically lacked a suitable expansion device, hindering its market attractiveness. As scroll expanders have been pointed out as strong potential candidates, performance correlations and pre-design maps based on a review and analysis of published experimental data are presented. A dimensionless approach based on the traditional Ns, Ds dimensionless numbers stemming from turbomachinery has been chosen for greater generality. In addition, the lubricating oil mass fraction effect on the scroll expander performance has been included. The generated maps contribute to accelerating the pre-design phases at the system and component level with beneficial effects for the overall development process. Basic geometry and size characteristics are considered as well, acknowledging their importance in micro-power embedded applications; these considerations are illustrated in a passenger car waste-heat recovery case study. Findings suggest that optimized scroll expanders may potentially reach very interesting nominal electric isentropic efficiencies (up to 80% for an oil lubricated scroll expander).

Introduction

Decentralized energy conversion is growing more and more since it is needed for transitioning towards low-carbon energy systems [1]. In this context, the significant potential of micro-power generation (<10kWe) based on low-temperature heat sources has been identified by various authors [2–5], while the Organic Rankine Cycle (ORC) has been widely studied and recognized as one of the leading candidates for such tasks [6–9]. Literature considers the expander device as one of the key technologies for both performance and commercial success of micro-scale ORC [10–14]. Hence, considerable attention has been paid to expanders [15,16], in particular to piston, rolling piston and scroll expanders. Piston and rolling piston expanders, although inexpensive, are mainly penalized due to the requirement of check valves and a limited lifetime. The scroll technology has received significant attention in research in recent years, reinforced by its success as a compressor in the refrigeration and air-conditioning industry. Since it is being mass produced already for these markets, this clearly proves its feasibility also in terms of cost [17,18]. Further, the scroll technology offers interesting volume ratios and efficiencies while maintaining acceptable manufacturing complexity [14,16,19].

Scroll systems can be classified according to several criteria. In terms of the relative motion between scroll involutes, the co-rotating and orbiting mechanisms are to be distinguished. In co-rotating scrolls, the two involutes rotate in a carefully synchronized manner. In the orbiting scroll case, one of the scroll plates remains stationary while the other follows an orbital motion. Co-rotating scroll machines have lagged behind orbiting scrolls in the compressor scroll market due to a series of technical difficulties mainly associated with the synchronization of the scroll volutes [20]. However, they are still a subject of research and study, in particular due to their tolerance to liquid injection [21]. In terms of the driving type: direct-

drive or open-drive systems are available. Hermetic and semi-hermetic systems belong to the direct-drive type, in which generator and expander are mounted on a single shaft avoiding the need for shaft seals. In hermetic and semi-hermetic systems, all of the elements required for the scroll operation are integrated inside a housing. These configurations are air-tight, thus avoiding working fluid leakage into the environment. The difference between hermetic and semi-hermetic systems is that the former cannot be opened without damaging the housing since it is a welded single piece, whereas the latter is accessible for maintenance [22]. Hermetic and semi-hermetic systems are commonly intended to be used in stationary applications where tightness during an extended lifetime is a priority. Scroll open-drive systems do not integrate the prime mover with the scroll expander on a single shaft and housing, thus allowing power transmission via a drive belt or equivalent mechanisms. The downside of open-drive systems is that refrigerant tightness can be compromised as the shaft seals degrade over time. Scroll expanders may be further categorized with respect to their internal kinematics. The kinematically rigid configuration constraints physical contact between orbiting and stationary scrolls through a dedicated guiding mechanism, thus allowing for operation without a lubricant. However, they are subject to more internal leakage, with respect to the compliant type [23]. In contrast, compliant scrolls provide the orbiting scroll with additional degrees of freedom, in both radial and/or axial directions, with the beneficial effect of increased robustness with regards to liquid ingestion and increased tightness [24,25]. Compliant orbiting scrolls require internal lubrication to avoid premature wear.

Modeling of scroll systems has been addressed by different authors, with proposed models ranging from empirical to deterministic ones [26]. For scroll expanders, empirical models have been mainly focusing on the expander isentropic efficiency and filling factor [27]. Such empirical models have commonly originated from calibrated semi-empirical models. Quoilin [28] proposed empirical logarithmic correlations based on a particular scroll expander test campaign. Lemort et al. [29] expressed the isentropic efficiency and filling factor of a particular scroll expander using polynomial regressions. Declaye et al. [30] proposed an isentropic efficiency parameterized expression inspired by Pacejka's equation whereas the filling factor was correlated through a linear regression based on rotor speed, supply pressure and pressure ratio. Mendoza et al. [32] correlated an experimentally identified leak area parameter from the semi-empirical model used by Lemort et al [33] to operating conditions of a specific scroll expander. Ibarra et al. [34] proposed the estimation of the mentioned leak area parameter for a specific scroll expander assuming a geometrical scaling law, without including the influence of operating conditions. Unfortunately, the proposed empirical models for scroll expanders are limited to a specific geometry and operating range. Hence, they cannot be used outside of the validated range for general design purposes without incurring significant errors. In contrast, deterministic models offer a more detailed scroll expander description in which the thermodynamic state during the expansion process is coupled with a spatial variable defining the scroll chamber geometry evolution. These models are of far wider applicability than calibrated semi-empirical models but are impractical to use for general pre-design purposes due to the requirement of a considerable number of detailed geometrical design parameters.

Nature of the Issue. In the context of expander selection for micro-scale ORC, general non-dimensional scroll expander performance maps are not available in the literature. Hence, the quick identification of the optimum scroll expander design for a given set of specifications is currently very difficult.

Goal and Objectives. The goal of this research is to achieve a general performance analysis and qualitative characterization of scroll expanders applied to micro-scale ORC. The objectives are: (1) to establish a methodology to determine the scroll expander performance based on a general semi-empirical model with correlated parameters from a literature data review. (2) To devise a unified set of design guidelines to determine qualitative scroll expander characteristics such as size and weight. (3) To apply the developed methodology for the scroll expansion device to a case study based on waste heat recovery for passenger cars.

The technological roadmap in this paper takes advantage of published experimental data using scroll expanders - which are mostly based on inverted commercial scroll compressor machines - along with the use of semi-empirical models. This procedure coupled to a non-dimensional representation allows to elaborate non-dimensional performance maps, size and weight correlations for scroll expanders.

1. Scroll expander analysis

1.1 Dimensionless performance maps

Dimensionless maps predict performance as a function of operating conditions and of a minimum number of variables, while covering a range as large as possible of machine sizes to be of practical interest. Experimentally validated simulation models offer the best trade-off for map reliability and range; however, these models become inaccurate, when used outside of their validated range. 0D models for scroll expanders are based on a classical volumetric machine description as presented by Kane [35]. The working fluid expansion is described as a two-step process as shown in Figure 1 (a): an isentropic expansion is followed by an expansion at constant machine volume. Loss mechanisms responsible for reducing isentropic efficiency are leakage $\mathbf{L_v}$, unadapted expansion losses $\mathbf{L_{ou}}$, pressure drops $\mathbf{\Delta P_{su}}$, heat exchange with ambient $\mathbf{\dot{Q}_{amb}}$ and mechanical losses $\mathbf{L_{mech}}$. The model presented in Figure 1 (a) requires 7 input variables (supply temperature $\mathbf{T_{su}}$, exit pressure $\mathbf{P_{ex}}$, rotor speed $\mathbf{N}$, working fluid, swept volume $\mathbf{V_{sw}}$ and built-in volume ratio $\mathbf{V_r}$) and 6 calibration parameters to compute the individual losses. The calibration parameters have to be determined experimentally. To overcome the explicit parameter calibration for each new scroll geometry or operating condition, and thus allowing the 0D model to be used in a general manner, two steps are undertaken. The first one regroups isentropic degradation mechanisms such as thermal losses $\dot{Q}_{amb}$ and pressure drops $\mathbf{\Delta P_{su}}$into a lumped loss term L_{lump}. The second step consists in the expression of the calibration parameters *uniquely* as a function of operating conditions and machine geometry. This dimensional reduction clearly results in a decrease in accuracy with respect to a dedicated calibrated model, however, a wider-reaching pre-design and rating tool is gained instead. The resulting reduced-dimension model in Figure 1 (b) needs the 7 same mentioned inputs but no additional experimental parameter determination is required. In addition, it expands the system boundary to account for electricity conversion (boundary SB_{III}).

$$\eta_{is,I} = \eta_v . \eta_{ou} . \eta_{lump} \quad (SB_I)$$
$$\eta_{is,II} = \eta_{is,I} \cdot \eta_{mech} \quad (SB_{II}) \qquad (1)\ (a,b,c)$$
$$\eta_{is,III} = \eta_{is,II} \cdot \eta_{elec} \quad (SB_{III})$$

According to Figure 1 (b) and Figure 2, the following isentropic efficiencies are defined, depending on the considered system boundary:

where $\eta_{is,I}$ is the isentropic efficiency considering the internal expander work: $E_{in} = \eta_{is,I}\, Y_{su,is}$ where $Y_{su,is} = \dot{m}_{su}\, \Delta h_{su,is}$ corresponds to the effective isentropic fluid power. By further considering the system's shaft power E_{mech}, $\eta_{is,II}$ is defined such that: $E_{mech} = \eta_{is,II}\, Y_{su,is}$. Finally, when the electrical conversion is of interest, the electrical output can be calculated as: $E_{elec} = \eta_{is,III}\, Y_{su,is}$.

The development of the generalized scroll performance map requires a simulation model free from experimental calibration for each new calculated point. Hence, the factors in Eq. 1 such as over-under expansion losses, volumetric efficiency, lumped losses and mechanical efficiency have to be computable solely with the model inputs. The efficiency factors and their modeling are explained in more detail:

Over-under expansion η_{ou}. The mismatch between imposed pressure ratio (operating conditions) and actual adapted pressure ratio achievable with the scroll's chamber geometry may lead to under/over expansion losses which can be predicted by a simple model presented by Lemort et al. [30]:

$$\eta_{ou} = \frac{\Delta h_{adap,is} + v_{adap}(P_{adap} - P_{ex})}{\Delta h_{su,is}} \tag{2}$$

Volumetric efficiency η_v. According to [36] the volumetric efficiency η_v for positive displacement machines can be expressed as follows:

$$\frac{1}{\eta_v} = 1 + \frac{\Psi\sqrt{r\,T_{su}}\,A\,G}{\pi\omega D} \tag{3}$$

where $\Psi \propto \sqrt{1 - 1/Er^2}$ embodies a leakage fluid velocity coefficient and Er is the expansion ratio; A is a dimensionless leak area, G a machine geometric characteristic, D the characteristic expander diameter and ω the rotational angular speed. Unfortunately, Eq. 3 requires detailed geometrical data (A and G), which are difficult to obtain or unavailable at pre-design stage. In order to avoid the need of dimensional expander data for predicting volumetric efficiency a set of non-dimensional parameters can be used as follows to non-dimensionalize Eq. 3:

$$\Pi_1 = \sqrt{1 - 1/Er^2} \qquad \Pi_2 = \frac{a_{su}}{\omega D^*} \tag{4}(a,b)$$

where Π_1 accounts for Ψ, and Π_2 for the $\frac{\sqrt{rT_{su}}}{\omega D}$ factor in Eq.3. Π_2 corresponds to the non-dimensionalized speed of sound at supply conditions relative to the scroll tip speed. Note that in the reference Eq. 3 the speed of sound of a fixed ideal gas is approximated by the numerator $\sqrt{rT_{su}}$, (r is the gas constant) whereas in the present investigation REFPROP has been used to calculate all of the used thermodynamics properties, including a_{su}. The definition of the diameter D^* used in the experimental data collection is a normalized scroll diameter such that:

$$\frac{\pi D^{*2}}{4} = \frac{(V_{sw}+V_{ex})}{b} = \frac{V_{sw}(1+Vr)}{b} \qquad [m^2] \tag{5}$$

where D^* corresponds to the diameter of a cylinder of height b and volume $V = V_{sw} + V_{ex}$. D^* has been employed instead of the scroll wrap diameter D , since the latter is only occasionally reported in the literature, whereas the geometric values needed to compute D^* are more accessible and provide a characteristic shape factor, since D^* condenses main scroll geometrical features such as V_{sw}, Vr and b into a single number. Note that the derived quantity D^{*2} is proportional to the product of the scroll pitch, the shape factor S_f and the crankshaft radius (see Appendix C). For sake of reduced dimensionality, the number $\Pi_B = \Pi_1 \cdot \Pi_2$ is introduced. A typical dimensionless power law expression stemming from Eq. 3 to be fitted with experimental data found in literature is given in Eq. 6:

$$\frac{1}{\eta_v} = 1 + c_0 * {\Pi_B}^{\alpha_b} \tag{6}$$

Note that Eq. 6 does not specifically take into account the effect of lubricating oil on the volumetric efficiency. Yet, its effect needs to be accounted for since it acts as a sealing agent between the scroll

involutes and is well known to influence the volumetric efficiency. In order to express this impact, an oil-to-void fraction ratio is proposed as follows:

$$\Pi_{vf} = \frac{\epsilon_{oil}}{\epsilon_f} = \frac{1-\epsilon_f}{\epsilon_f} \quad 0 < \epsilon_f \leq 1 \tag{7}$$

dwhere the void fraction ϵ_f is defined as:

$$\frac{1}{\epsilon_f} = 1 + \chi \cdot \frac{\rho_{ref}}{\rho_{oil}} S \tag{8}$$

With $\chi = \frac{x_{oil}}{x_{ref}}$ the oil-to-refrigerant mass fraction ratio and S the slip ratio defined according to [37]:

$$S = K + (1-K)\left[\frac{\left(\frac{\rho_{oil}}{\rho_{ref}}\right) + K \cdot \chi}{1 + K \cdot \chi}\right]^{0.5} \quad [-] \tag{9}$$

where K is the fraction of liquid (oil) entrained in the refrigerant as droplets. A value of 0.4 is commonly used [37]. The oil density is estimated according to Eq. 10, a density correlation for an Alkylbenzene oil [50] (Tridecylbenzene) used in ORC applications [51].

$$\rho_{oil} = 1055 - 0.7 \cdot T_{su} \qquad \left[\frac{kg}{m^3}\right] \tag{10}$$

The void fraction number Π_{vf} defined above could be easily included as a factor or a quotient in the rearranged dimensionless power law:

$$\frac{1}{\eta_v} - 1 = \frac{c_0 \cdot {\Pi_B}^{a_1}}{\Pi_{vf}^{a_2}} \tag{11}$$

Unfortunately, such an expression would lead to an incoherent volumetric efficiency in the absence of oil since:

$$x_{vf} = 1 \leftrightarrow \Pi_{vf} = 0, \quad \rightarrow \eta_v \approx 0,$$

Therefore, a constant c_1 is introduced to appropriately account for the oil-free cases such that:

$$\frac{1}{\eta_v} - 1 = \frac{c_0 \cdot \Pi_B^{a_1}}{c_1} \tag{12}$$

Writing $c_2 = c_1^{1/a_2}$, noting that $c_2 \ll \Pi_{vf}$ and considering the fact that the term Π_{vf} vanishes under oil free operation, allows to reduce (11) and (12) into a single expression for all cases:

$$\frac{1}{\eta_v} \sim 1 + \frac{c_0 \cdot \Pi_B^{a_1}}{(c_2 + \Pi_{vf})^{a_2}} \tag{13}$$

In order to identify the parameters of Eq. 13 a curve fitting of experimental data points collected in the literature and summarized in Appendix A and B is performed in two steps. The experimental data used for fitting the parameters (c_0, a_1, a_2) of Eq. 13 include various working fluids (N_2, Air, NH_3, R245fa, R134a, and R123), both compliant (cp.) and kinematically constrained (k.c) scroll expanders, and operation with and without oil. The constant c_1 is determined for the oil-free case ($x_{ref} = 1 \rightarrow \Pi_{vf} = 0$) with points corresponding to the R123 oil-free study [33]. The reason inorganic fluids have been included in the fitting is to take advantage of the dimensionless nature of Eq. 13, which suggests it is applicable independently of the working fluid. In addition, the use of inorganic fluids provides further insights on the scroll expander performance as it is discussed in the following lines.

Table 1 summarizes the statistical evaluation quality for Eq. 13, including the interval of confidence for estimators and the R^2 model coefficient of determination. Figure 3 represents the volumetric efficiency η_v according to the obtained fit in Eq. 13 as a function of Π_B and void fraction ϵ_f (and thus Π_{vf} as a parameter) Solid ϵ_f isolines conform to the range of reported experimental ϵ_f values, including oil fraction uncertainties, while dashed lines extend beyond the experimental ϵ_f values. The experimental volumetric efficiency of the collected experimental points is plotted on top of the identified reduced-dimension model. In order to visually inspect the model accuracy against the experimental data points Figure 4 (a) compares model training data with volumetric efficiency values obtained by the fitted Eq. 13. The results clearly suggest that higher volumetric efficiency can be achieved both through increased oil fractions and a higher Π_B, which corresponds to a higher product of rotor speed and D^*. Good agreement is achieved for R245fa and ammonia. Larger discrepancies appear for Nitrogen and for the Air I data sets. This is most likely due to the high uncertainty level in reported oil fraction values of 17.7 - 90.7% for Nitrogen and up to 40% of relative error for Air I data sets. Note, that the authors of these two studies explicitly varied the oil fraction in order to measure its impact on the scroll expander performance, providing an interesting range of oil mass fractions at different operating conditions.

Figure 4 (b) shows the accuracy of Eq. 13 by comparing it to experimental data points which were not part of the model training data and for which oil mass fractions have been inferred from Figure 3, since the experimental oil fractions were not availabl Rough estimations of constant oil fraction values were imposed: 0.5% and 1.7 % for Air II and R134 data sets respectively, suggesting conservative oil mass fractions were used.

Regarding the kinematically constrained data set for R123, oil lubrication was reported, however, no details are given on its mass fraction. Nonetheless, assuming standard oil mass fractions in the range of 0.5-5%, Figure 3 suggests that the addition of oil does not have the same beneficial effect on the volumetric efficiency as for compliant scroll expanders. As a matter of fact, the data points with oil-lubrication perform only slightly better than the oil-free cases. This is due to the fact that the oil sealing capability results from the centrifugal sealing effect present in compliant scrolls, which is neutralized in the kinematically constrained configuration as noted by Peterson et al. [38].

The results in Figure 4 suggest a good agreement between the experimental data and the reduced order volumetric efficiency model for both inorganic and organic fluids, across a wide range of operating conditions and scroll geometries. Hence, the selected approach based on the identified non-dimensional groups is validated.

Lumped losses η_{lump}. Lumped losses collect pressure losses, thermal losses, and other degradations occurring during the expansion process. With the available experimental data, they can be defined as follows:

$$\eta_{lump} = \frac{\eta_{is,II,exp}}{\eta_{v,exp} \cdot \eta_{ou} \cdot \eta_{mech,exp}} \tag{14}$$

It is suggested, however, that the largest contributors to these losses are the pressure drops [22,28,33], which can be represented as an expansion through a convergent nozzle with a given throat area [33]. According to [33], for a stationary and isentropic nozzle, the kinetic energy due to a pressure drop is expressed as follows:

$$C^2/2 = \begin{cases} \Delta h_{is} & \text{if} \quad \Delta h_{is} < \Delta h_{is,lav} \\ \Delta h_{lav} & \text{if} \quad \Delta h_{is} > \Delta h_{is,lav} \end{cases} \tag{15}$$

where $\Delta h_{is,lav}$ is the isentropic enthalpy drop at choked conditions (Laval point). As a consequence, the velocity in a convergent nozzle can be expressed as follows:

$$\frac{C^2}{2} = f_0(\Delta h_{is}, \Delta h_{is,lav}) \tag{16a}$$

By dimensional analysis, two Π-groups are defined $\Pi_{\Delta P} = \frac{C^2/2}{\Delta h_{is}}$, $\Pi_{lav} = \frac{\Delta h_{is,lav}}{\Delta h_{is}}$ such that:

$$\Pi_{\Delta P} = \frac{C^2/2}{\Delta h_{is}} = f_1\left(\frac{\Delta h_{is,lav}}{\Delta h_{is}}\right) = f_1(\Pi_{lav}) \tag{16b}$$

Where $\Pi_{\Delta P}$ is a metric of the relative energy loss due to a pressure drop. Therefore, the lumped efficiency η_{lump}, which is mainly driven by the pressure drop, has a functional dimensionless dependence with the number $\Pi_{\Delta P}$. Since from a phenomenological point of view the lumped efficiency is also a function of the rotor speed, the volumetric flow and the machine dimensions, the specific speed $Ns = \frac{\omega \cdot \dot{V}^{0.5}}{\Delta h_{is}^{0.75}}$ and the machine specific diameter $Ds = \frac{D^* \cdot \Delta h_{is}^{0.25}}{\dot{V}^{0.5}}$ stemming from the turbomachinery analysis are introduced:

$$\eta_{lump} = f_2(\Pi_{\Delta P}, N_s, D_s) \tag{17a}$$

Combining Eq. 16b and Eq. 17a the lumped efficiency can be equivalently expressed as a function of Π_{lav}:

$$\eta_{lump} = f_3(\Pi_{lav}, N_s, D_s) \tag{17b}$$

In order to further decrease the number of dimensions, the number $D_{s,lav} = D_s \cdot \Pi_{lav}^{0.25} = \frac{D^* \cdot \Delta h_{is,lav}^{0.25}}{\dot{V}^{0.5}}$ is defined. The dimensionless correlation based on a classical power law to be fitted is finally given as follows:

$$\frac{1}{\eta_{lump}} = 1 + 10^{b_0} N_s^{m_1} D_{s,lav}^{m_2} \tag{18}$$

Experimental data from five studies shown in Appendix A and B, for which isentropic efficiency values in the sense of $\eta_{is,II}$, $\eta_{v,exp}$ and $\eta_{mech,exp}$, are available with sufficient accuracy, allow the identification of the fitting parameters of Eq. 18 presented in Table 2. Figure 5 (a) shows the penalizing effect of increasing rotational speed for a given Ds value, which is consistent with the observation that pressure losses increase with rotor speed, in contrast to volumetric efficiency which increases with Ns (or rotor speed). The lumped losses do not integrate the effect of oil nor distinguish between the kinematically constrained from compliant scroll case. As suggested by Figure 5 (b), the compliant, oil lubricated experimental data sets (N_2, Air I, NH_3 and R245fa) present a satisfactory agreement while the oil-free kinematically constrained data set (R123) shows a larger error spread, remaining nonetheless, within a 16% relative error band.

Mechanical losses L_{mech} The mechanical losses can be estimated with good accuracy based on the scaling law proposed by Lemort et al. [33]:

$$L_{mech} = \omega \cdot \tau \cdot \left(\frac{V_{sw}}{V_{sw,ref}}\right)^{2/3} [W] \text{ and } \eta_{mech} = 1 - \frac{L_{mech}}{Y_{su,is}\eta_{is,I}} \qquad (19)(a,b)$$

with $\tau = 0.47$ [N. m] and $V_{sw,ref} = 36.54$ [cm^3]

Scroll design map. Assuming adapted expansion, the fitted expressions of the volumetric efficiency (Eq. 13) and lumped efficiencies (Eq. 18) allow to predict the achievable isentropic efficiency as a function of Ns and Ds and to plot a generalized scroll design map based on the ranges established in Table 3. Figure 6 shows predicted isentropic efficiency contours as a function of Ns, Ds for a scroll expander operated in adapted expansion (η_{ou} = 1) with oil lubrication at an oil mass fraction of 2%. At large Ns-values the isentropic efficiency is limited due to high lumped losses (mainly pressure losses). At small Ns-values, it is the low volumetric efficiency restricting the isentropic efficiency. This competing behavior of the two loss mechanisms with respect to the scroll expander rotor speed has been highlighted by Quoilin [28]. However, it is interesting to note, that the optimum trade-off between these two loss mechanisms shifts with Ds. Note that expander efficiency calls for larger Ds values at low specific speeds, and conversely, lower Ds at higher specific speeds. The overall optimum efficiency zone, is concentrated in the high-Ns low-Ds region, which suggests that scroll expanders are expected to perform better when operated at high rotor speeds with reduced characteristic diameter and larger wrap heights. For an optimum shaft power or optimum efficiency $\eta_{is,II}$, the penalty of the mechanical torque losses of Eq. 19 has to be included in the calculation of the optimum Ns-Ds pair.

As a final remark, the effect of refrigerant kinematic viscosity on the isentropic efficiency of scroll expanders was further investigated based on a machine Reynolds number $\left(\mathrm{Re} = \frac{\omega D}{\mu}\right)$ with the available data. No concluding statistical significance was found. This is probably due to the fact that in the studied data range, the Re number variance is dominated by the inertial factor (which is already included in the Π_B number). This outcome suggests that the refrigerant viscosity influence on the scroll expander performance, within the ORC typical operating conditions, can be neglected.

Model limitations. The fitting of the volumetric efficiency and lumped losses is based on a limited number of published experimental data, which may be biased by the accuracy in the reported machine geometries and measurement procedures. Nonetheless, great care has been applied in the selection of published data and only measurements with a satisfactory number of indicated variables have been considered in this work. Further, the model dimension reduction based on the similarity concept, the fitting procedure with experimental data and the lumping of various loss mechanisms are inherently reducing the model accuracy. Although the agreement between model prediction and experimental data is remarkable, particular care needs to be taken when extrapolating outside of the boundary of the original data, which is summarized in the Appendix A and B.
In addition, the majority of scroll expander data used for the model fitting is based on commercial scroll compressors, which do not necessarily coincide with optimum expander configurations. It follows that the scroll expander design maps are limited to the current scroll compressors state-of-the-art.
However, given the model limitations and considering the overall coherence of results, it can be stated that the presented dimensionless approach yields a robust methodology to capture the described phenomena based on a very limited amount of information. The satisfactory agreement of the obtained results suggests that the hypotheses made are adequate for generalized scroll expander pre-design tool.

1.2 Scroll system mass and volume

In order to extend the scroll expander design maps, insights with respect to mass and volume are investigated. These criteria are of relevance for applications where size and weight come at a premium, in particular in the transportation or aerospace industry. Scroll expander size and mass depend not only on geometry but also on the driving type: open or direct-drive. The volume and mass of scroll expanders may be estimated from existing scroll compressor systems since both systems are virtually reversible.

Open-drive systems. The scroll total mass and volume, including the weight of the transmission clutch are presented as a function of the scroll chamber volumes ($V_{sc} = V_{sw} + V_{ex}$) in Figure 7. The data points

correspond to scroll systems, which have been optimized for lightness and compactness since they were designed for passenger cars [40]. Mass and volume correlations for open drive systems are given in Eq. 20. In order to discount the clutch, a mass of 1.9 kg and a volume of approximately 0.4 L can be subtracted. (Squared points in Figure 7).

$$m_{tot} = 0.0151 \cdot V_{sc} + 3.77\ [kg] \qquad V_{tot} = 2.29 \cdot V_{sc} + 4.23 \cdot 10^3\ [cm^3] \qquad (20)(a,b)$$

Direct-drive systems. Hermetic and semi-hermetic scroll systems integrate the prime mover and all the subsystems needed to run the compressor, including oil management. For these systems, the total weight and volume is mainly driven by the rated power of the prime mover, as represented in Figure 8.

$$m_{tot} = 18.33 \cdot E_{elec}^{0.522}\ [kg] \quad V_{tot} = 1.39 \cdot 10^4 \cdot e^{(0.0187 \cdot m_{tot})}\ [cm^3] \qquad (21)(a,b)$$

Data points (Copeland ZB and ZH series) are based on the most compact and lightest scroll series identified by comparing products of leading compressor manufacturers. Figure 7 and 8 suggest that the total scroll system mass and volume can be estimated as a function of the rated power, since the variation in the scroll chamber mass with the increase of total chamber volume V_{sc} is negligible with respect to the system overall dimensions. Eq. 21 (a,b) shows the obtained fits for the scroll system total mass m_{tot} as a function of the rated electric power E_{elec} (in kW) and the scroll system total volume V_{tot} (in cm^3) as a function of the former.

Based on geometrical data from scroll expanders presented in the Appendix A, an empirical relationship between the swept volumes, volumetric ratios and wrap heights has been established as follows:

$$D^* = 0.03387 \cdot V_o + 4.213\ [cm] \qquad (22)$$

where D^* is defined in Eq. 5 and V_o corresponds to the scroll outer chamber in cm^3. Depending on the original scroll configuration it may be the swept V_{sw} or the exhaust V_{ex} chamber volume. Eq. 22 being established across different scroll manufacturers and models highlights a design trend, which is neither universal nor necessarily the optimum design for scroll expanders. It contributes, however, to the description of scroll geometries currently available on the market and can therefore be used as a reference. Indeed, once the swept volume and volumetric ratio have been defined for a given operation, combining Eq. 22 and Eq. 5 allows deducing the scroll wrap height b As a reference, Orosz provides $b = 7 \cdot V_o^{0.58}$ mm with V_o in cm^3 based on an empirical fitting [41].

2. Case study

The following section provides an example where the Ns-Ds map for scroll expanders introduced in this paper are used to pre-design a micro ORC system. The selected case study is a waste heat recovery application from the internal combustion engine exhaust gases of a passenger car. The ORC is composed of a feed pump, which brings the refrigerant to a high-pressure level, an evaporator harnessing energy from the exhaust gasses, a scroll expander and a condenser, which condenses the refrigerant with ambient air. Table 4 summarizes the boundary conditions of the cycle for the scroll expander, based on work for a similar application presented by Rosset et al. [42]. A 5K pump inlet subcooling is imposed to avoid cavitation. Finally, a variable pressure ratio ranging from 2 to 8 is used as a sensitivity analysis parameter.

The scroll expander performance with the imposed cycle conditions is first examined with indicators based on efficiency and power. These indicators are further completed with rotor speed and size such as normalized diameter, mass and volume. Rotor speeds, which are intrinsically related to the expander size, are decisive for a number of engineering choices such as materials, bearing design or the eventual need of an electrical converter.

The volumetric flow and the isentropic enthalpy drop are calculated through the thermodynamic cycle subject to the boundary conditions presented in Table 4. Once the volumetric flow and the isentropic enthalpy drop within the expansion process are computed, the optimal rotor speed ω_{opt} and the scroll optimal diameter D^*_{opt} are retrieved from the Ns-Ds values yielding the best isentropic efficiency in terms of the $\eta_{is,II}$ definition.

The overall generator efficiency is set to constant values as presented in Table 5 and is composed of an electric converter efficiency η_{cv} and of an induction generator efficiency $\eta_{gen,ind}$. The mechanical efficiency is computed according to Eq. 19.

The scroll expander is defined as a compliant semi-hermetic machine operating with 2% mass fraction of oil. The scroll case feasibility constraints are listed in Table 3. According to these, an optimal characteristic diameter D^* -where the wrap height b and swept volume V_{sw} vary independently within the geometrical constrains- can be found. For the scroll expander, a second case is analyzed where the scroll expander exhaust (outer) chamber volume is linked to the normalized diameter D^* such as previously identified in the case of commercial scroll compressors shown in Figure 9 and expressed in Eq. 22. Compared to the first case, this second one represents a constrained optimization in the sense that the normalized diameter is not independent of the swept volume V_{sw} anymore.

The resulting performance indicators of the optimized expanders are presented in Figure 10. The first observation is a significant performance shift between the constrained scroll shape model and the optimum shape case. The reason is that the maximum efficiency line projected onto the Ns-Ds plane for the constrained model lies below the theoretical maximum efficiency line, because of the added constraint, reaching thus only mediocre efficiencies. On the contrary, the best efficiency line for the unconstrained normalized diameter is able to reach higher values, limited, however, by other geometrical constraints such as the maximum wrap height b at low P_r or the maximum V_r at high P_r (see Figure 12).

In terms of isentropic efficiency $\eta_{is,III}$, the optimum scroll expander ranges from 70 % at the lowest $\overline{P_r}$ and peaks at 80 % for a pressure ratio close to 6.8 before falling by the penalizing effect of unadapted expansion due to the maximum allowed volumetric ratio (Figure 10 and Figure 12). Shaft powers achieve 2.7 kW for the optimum scroll expander while the constrained scroll only approaches 1.4 kW. Finally, the maximum ORC net power and cycle thermal efficiency are close to 2.2 kW and 11 % for the optimum scroll case. The constrained scroll yields 1.2 kW maximum ORC net power and ~6% maximum cycle thermal efficiency.

Figure 11 presents the evolution of optimal rotor speeds, normalized diameters, as well as expander mass and volume, as a function of the installed pressure ratio. The rotor speeds are limited below 4 krpm by the effect of the lumped losses, (mainly pressure drop) at higher Ns values (Figure 5) and the activation of the minimum scroll normalized diameter constraint of 50 mm. The optimum swept volume of the scroll expander initially reduces steeply as the rotor speed increases (Figure 11), to subsequently moderate the decrease as the scroll diameter reaches a minimum (Figure 12). The swept volume continues its decrease despite a lowering rotor speed because of the reduced volumetric flow at the expander supply with higher P_r. The volume decrease is then driven by a scroll wrap height decrease without reaching the minimum constraint value of 20 mm.

From the presented scroll expander analysis and case study, the following conclusions can be drawn:

1. For given operating conditions, scroll expander performance is closely related to machine geometry and rotor speed. The comparison suggests that the expander normalized diameter, plays a significant role in the scroll expander performance.
2. The predicted performances and geometries are based on the premise of maximum efficiency at nominal operation. This implies that additional design or engineering constraints will downgrade the expected efficiency of the expanders. Consequently, a more detailed simulation model will yield a closer-to-reality performance.
3. Scroll expanders operate best when using compliant mechanisms and lubricating oil. The results suggest over 10 points of volumetric efficiency gain when operated in the high efficiency region since oil acts as a sealing agent.
4. The presented study simplifies the pre-design task to a set of single best-operating-points, but a more complete study should consider the expander and performance over a full operating range (off-design). In this regard, scroll expanders are penalized by both unadapted expansion and pressure losses.

3. Conclusion

The present investigation offers a synthesis of the scroll technology used as expansion device for micro-ORC and contributes to the generation of scroll performance maps by combining semi-empirical models with a range of published experimental data. The analysis of data shows that better scroll expander performance is expected from compliant mechanisms with respect to kinematically constraint systems, mainly due to more pronounced leakage of the latter. The oil mass fraction effect on volumetric efficiency can be accounted for in terms of void fraction; it is observed to increase sealing over 10 points compared to oil-free operation. The use of traditional dimensionless numbers Ns, Ds appears to be adequate to characterize scroll expanders as suggested by Balje, noting nonetheless the opportunity to further refinement by integrating more detailed simulation models. The use of a normalized diameter D^* was proposed for the scroll expander Ds definition, integrating key geometrical parameters such as the volume ratio V_r and the scroll wrap height b. A strong penalty related to an inadequate scroll geometry for given operating conditions was observed, suggesting that an adapted geometry should provide improvement opportunities in future scroll expander designs.

Additionally, mass and volume correlations for scroll expander systems were provided, based on commercial scroll compressors, which can be of considerable importance depending on the targeted application.

The novel performance maps have been applied to a passenger car waste heat recovery case study suggesting maximum isentropic electrical efficiencies at design point of 80 %, on the condition that the scroll expander is run with lubricating oil. A more detailed study considering expander performance over a range of off-design conditions would provide further useful insights about the considered expanders.

Nomenclature

Symbol	Meaning	Unit
a	speed of sound	m/s
A	dimensionless leak area	-
b	height	m
C	fluid velocity	m/s
D	expander diameter	m
Ds	specific diameter	-
E	technical power	W
Er	expansion ratio	-
G	scroll geometric parameter	-
h	enthalpy	kJ
K	fraction of liquid	-
L	power loss/dissipation	W
m	mass	kg
N	rotor speed	rpm
Ns	specific speed	-
P	pressure	Pa
$\dot{Q}$	heat flow rate	W
r	specific gas constant	J kg^{-1} K^{-}
Re	Reynolds number	-
S	slip ratio	-
T	temperature	K
V	volume	m^3
$\dot{V}$	volumetric flow	m^3/s
x	mass fraction	-
Y	fluid power	W

Greek letter	Meaning	Unit
η	efficiency	-
ϵ_f	void fraction	-
μ	kinematic viscosity	Pa.s
Π_1	Dimless. approx of Ψ	Pa
Π_2	dimless fluid speed of sound at supply conditons	-
Π_B	$\Pi_1 \cdot \Pi_2$	-
$\Pi_{\Delta P}$	Relative kin. energy loss due to pressure drop.	-
Π_{lav}	$\frac{\Delta h_{is,lav}}{\Delta h_{is}}$	-
Π_{vf}	$\frac{1-\epsilon_f}{\epsilon_f}$ oil-to void fraction ratio	-
ρ	Density	$kg.m^{-3}$
τ	torque	N.m
χ	mass fraction ratio	-
Ψ	leakage fluid coefficient	-
ω	rotor speed	rad/s

Subscripts

I	before mechanical loss (See Fig 1;Fig2)
II	after mechanical loss
III	after electrical loss
adap	Adapted
amb	Ambient
cond	Condensation
ex	Exhaust
exp	Experimental
gen	electric generator
in	Inlet
ind	Induction
is	Isentropic
lav	de Laval (Point)
lump	lumped(loss)
mech	mechanical
oil	scroll volute lubricating oil
ou	over/under expansion
r	ratio
ref	reference
rot	rotor
rs	reference scroll
sc	scroll chambers total volume

Acronyms

cp.	compliant
k.c.	kinematically constrained
ORC	Organic Rankine Cycle
SB	System Boundary

Figure Captions

Figure 1 (a) Original 0D scroll expansion model. (b) Simplified model with extended system boundaries.

Figure 2 Scroll expander Sankey diagram for simplified scroll model of Figure 1 (b).

Figure 3 Volumetric efficiency based on Eq. 13 as a function of Π_B and of the void fraction ϵ_f(lines). Experimental scroll expander data out of literature is plotted for comparison (points) for the various working fluids, and scroll concepts (compliant and kinematically constrained).

Figure 4 (a) Accuracy of calculated volumetric efficiency η_v (Eq. 13) against training data. (b) Accuracy of predicted η_v against experimental data not included in the training set. (But x_{oil} rough estimation based on Figure 3).

Figure 5 η_{lumped} based on the identified Eq. 18 and the comparison with experimental data as a function of specific speed Ns.

Figure 6 Scroll isentropic efficiency contours for adapted expansion as a function of Ns, Ds with normalized scroll diameter D* and oil mass fraction x_{oil}= 0.02.

Figure 7 Open-drive scroll system total mass m_{tot} (a) and volume V_{tot} (b) as function of total scroll chamber volume V_{sc}.

Figure 8 Direct-drive scroll system mass (a) and total volume (b) as a function of scroll total chamber volume according to manufacturer.

Figure 9 Normalized scroll diameter fit based on Eq. 22 as a function of scroll outer chamber volume Vo according to commercial compressors from Appendix A.

Figure 10 Performance indicators for ORC and scroll expanders for the waste heat recovery case study for passenger cars as a function of pressure ratio.

Figure 11 Scroll expander rotational speed and system sizing comparison under case study conditions as a function of pressure ratio.

Figure 12 Scroll expanders best theoretical geometries under imposed operating conditions with varying pressure ratio.

4. Appendices

4.1 Appendix A – Scroll Geometrical Data

Table A-1 Scroll expander geometrical data.

4.2 Appendix B – Scroll Expanders Operating Data

Table B-1 Scroll expander geometrical data.

4.3 Appendix C – Derivation of D*, the normalized scroll diameter

Based on the basic scroll geometry definition, it is possible to highlight the relationship between the scroll chamber volumes and height to the scroll pitch and crank radius.

$$\frac{\pi D^{*2}}{4} = \frac{V_{sw} + V_{ex}}{b} \qquad AC(1) = \text{Eq. } (5)$$

By inspecting $AC(1)$, one can see that D* has the dimension of a length [m] and corresponds to the diameter of the basis of a cylinder of total volume $V_{sw} + V_{ex}$ and height b. Critically analyzing the relationship of the characteristic scroll device dimension and leakage, the sought dimension should reflect the length with which the sealing force varies. The crankshaft radius is a good indicator since the sealing force is proportional to the crankshaft radius. A machine shape factor reflecting for instance, the ratio of radial to flank leakage, would complement the relationship we are trying to establish. This shape factor is determined by the ratio of the scroll height and the volumes of the suction and exhaust chambers (V_r the built-in volume ratio) and the number of scroll wraps N.

The dependence of D^* with the crankshaft radius and the scroll shape factor can be verified with the basic scroll geometry definition with the compressor nomenclature [49]:

$$V_{sw} = \pi\, p(p - 2t)b(2N - 1) \qquad AC(2)$$

$$V_r = \frac{V_{sw}}{V_{ex}} \qquad AC(3)$$

Where p is the scroll pitch and N the number of scroll wraps.

Combining Eq. AC (1-3) yields:

$$\frac{V_{sw} + V_{ex}}{b} = \frac{\pi D^{*2}}{4} = (2N - 1)\left(\frac{V_r + 1}{V_r}\right) * p(p - 2t)\pi \qquad AC(4)$$

Therefore,

$$D^{*2} \propto S_f * p(p - 2t) = S_f \cdot p \cdot r_{crank} \qquad AC(5)$$

The shape factor is represented by the product: $S_f = \frac{V_r+1}{V_r}(2N\text{-}1)$

Thus, the derived quantity D^{*2} is proportional to the product of the scroll pitch, the shape factor S_f and the crankshaft radius.

5. Bibiography

[1] Alstone P, Gershenson D, Kammen DM. Decentralized energy systems for clean electricity access. Nat Clim Chang 2015;5:305–14. doi:10.1038/nclimate2512.

[2] Kang SH, Chung DH. Design and experimental study of organic Rankine cycle and radial turbine. Proc ASME Turbo Expo 2010 2011;41:1–7. doi:10.1115/GT2011-46152.

[3] Bracco R, Clemente S, Micheli D, Reini M. Experimental tests and modelization of a domestic-scale ORC (Organic Rankine Cycle). Energy 2013;58:107–16. doi:10.1016/j.energy.2012.12.016.

[4] Wei D, Lu X, Lu Z, Gu J. Dynamic modeling and simulation of an Organic Rankine Cycle (ORC) system for waste heat recovery. Appl Therm Eng 2008;28:1216–24. doi:10.1016/j.applthermaleng.2007.07.019.

[5] Peris B, Navarro-Esbrí J, Molés F, González M, Mota-Babiloni A. Experimental characterization of an ORC (organic Rankine cycle) for power and CHP (combined heat and power) applications from low grade heat sources. Energy 2015;82:269–76. doi:10.1016/j.energy.2015.01.037.

[6] Shengjun Z, Huaixin W, Tao G. Performance comparison and parametric optimization of subcritical Organic Rankine Cycle (ORC) and transcritical power cycle system for low-temperature geothermal power generation. Appl Energy 2011;88:2740–54. doi:10.1016/j.apenergy.2011.02.034.

[7] Vetter C, Wiemer H-J, Kuhn D. Comparison of sub- and supercritical Organic Rankine Cycles for power generation from low-temperature/low-enthalpy geothermal wells, considering specific net power output and efficiency. Appl Therm Eng 2013;51:871–9. doi:10.1016/j.applthermaleng.2012.10.042.

[8] Schuster A, Karellas S, Aumann R. Efficiency optimization potential in supercritical Organic Rankine Cycles. Energy 2010;35:1033–9. doi:10.1016/j.energy.2009.06.019.

[9] Le VL, Feidt M, Kheiri A, Pelloux-Prayer S. Performance optimization of low-temperature power generation by supercritical ORCs (organic Rankine cycles) using low GWP (global warming potential) working fluids. Energy 2014;67:513–26. doi:10.1016/j.energy.2013.12.027.

[10] Qiu G, Liu H, Riffat S. Expanders for micro-CHP systems with organic Rankine cycle. Appl Therm Eng 2011;31:3301–7. doi:10.1016/j.applthermaleng.2011.06.008.

[11] Bao J, Zhao L. A review of working fluid and expander selections for organic Rankine cycle. Renew Sustain Energy Rev 2013;24:325–42. doi:10.1016/j.rser.2013.03.040.

[12] Mathias J a., Johnston JR, Cao J, Priedeman DK, Christensen RN. Experimental Testing of Gerotor and Scroll Expanders Used in, and Energetic and Exergetic Modeling of, an Organic Rankine Cycle. J Energy Resour Technol 2009;131:12201. doi:10.1115/1.3066345.

[13] Quoilin S, Broek M Van Den, Declaye S, Dewallef P, Lemort V. Techno-economic survey of organic rankine cycle (ORC) systems. Renew Sustain Energy Rev 2013;22:168–86. doi:10.1016/j.rser.2013.01.028.

[14] Imran M, Usman M, Park BS, Lee DH. Volumetric expanders for low grade heat and waste heat recovery applications. Renew Sustain Energy Rev 2016;57:1090–109. doi:10.1016/j.rser.2015.12.139.

[15] Badr O, Naik S, O'Callaghan PW, Probert SD. Expansion machine for a low power-output steam Rankine-cycle engine. Appl Energy 1991;39:93–116. doi:10.1016/0306-2619(91)90024-R.

[16] Lemort V, Guillaume L, Legros A, Declaye S, Quoilin S, Lemort V, et al. A comparison of piston, screw and scroll expanders for small- scale Rankine cycle systems. Proc. 3rd Int. Conf. Microgeneration Relat. Technol., 2013.

[17] Clemente S, Micheli D, Reini M, Taccani R. Energy efficiency analysis of Organic Rankine Cycles with scroll expanders for cogenerative applications. Appl Energy 2012;97:792–801. doi:10.1016/j.apenergy.2012.01.029.

[18] Colonna P, Casati E, Trapp C, Mathijssen T, Larjola J, Turunen-Saaresti T, et al. Organic Rankine Cycle Power Systems: From the Concept to Current Technology, Applications, and an Outlook to the Future. J Eng Gas Turbines Power 2015;137:100801. doi:10.1115/1.4029884.

[19] Qiu G, Liu H, Riffat S. Expanders for micro-CHP systems with organic Rankine cycle. Appl Therm Eng 2011;31:3301–7. doi:10.1016/j.applthermaleng.2011.06.008.

[20] Iglesias A, Favrat D. Innovative isothermal oil-free co-rotating scroll compressor-expander for energy storage with first expander tests. Energy Convers Manag 2014;85:565–72. doi:10.1016/j.enconman.2014.05.106.

[21] Mendoza LC, Lemofouet S, Schiffmann J. Testing and modelling of a novel oil-free co-rotating scroll machine with water injection. Appl Energy 2017;185:201–13. doi:10.1016/j.apenergy.2016.10.089.

[22] Song P, Wei M, Shi L, Danish SN, Ma C. A review of scroll expanders for organic rankine cycle systems. Appl Therm Eng 2015;75:54–64. doi:10.1016/j.applthermaleng.2014.05.094.

[23] Wang H, Peterson RB, Herron T. Experimental performance of a compliant scroll expander for an organic Rankine cycle. Proc Inst Mech Eng Part A J Power Energy 2009;223:863–72. doi:10.1243/09576509JPE741.

[24] Bell IH, Lemort V, Groll EA, Braun JE, King GB, Horton WT. Liquid flooded compression and expansion in scroll machines - Part II: Experimental testing and model validation. Int J Refrig 2012;35:1890–900. doi:10.1016/j.ijrefrig.2012.07.008.

[25] Afjei T, Suter P, Favrat D, Afjci T, Suter2 P, Fawul D. Experimental Analysis of an Inverter-Driven Scroll Compressor with Liquid Injection n.d.

[26] Lemort V. Contribution to the characterization of scroll machines in Compressor and Expander modes 2008:307.

[27] Hu D, Li S, Zheng Y, Wang J, Dai Y. Preliminary design and off-design performance analysis of an Organic Rankine Cycle for geothermal sources. Energy Convers Manag 2015;96:175–87. doi:10.1016/j.enconman.2015.02.078.

[28] Quoilin S. Sustainable energy conversion through the use of Organic Rankine Cycles for waste heat recovery and solar applications. University of Liège (Belgium, 2011), 2011.

[29] Lemort V, Declaye S, Quoilin S. Experimental characterization of a hermetic scroll expander for use in a micro-scale Rankine cycle. Proc Inst Mech Eng Part A J Power Energy 2012;226:126–36. doi:10.1177/0957650911413840.

[30] Declaye S, Quoilin S, Guillaume L, Lemort V. Experimental study on an open-drive scroll expander integrated into an ORC (Organic Rankine Cycle) system with R245fa as working fluid. Energy 2013;55:173–83. doi:10.1016/j.energy.2013.04.003.

[31] Mendoza LC, Ayou DS, Navarro-Esbrí J, Bruno JC, Coronas A. Small capacity absorption systems for cooling and power with a scroll expander and ammonia based working fluids. Appl Therm Eng 2014;72:258–65. doi:10.1016/j.applthermaleng.2014.06.019.

[32] Mendoza LC, Navarro-Esbrí J, Bruno JC, Lemort V, Coronas A. Characterization and modeling of a scroll expander with air and ammonia as working fluid. Appl Therm Eng 2014;70:630–40. doi:10.1016/j.applthermaleng.2014.05.069.

[33] Lemort V, Quoilin S, Cuevas C, Lebrun J. Testing and modeling a scroll expander integrated into an Organic Rankine Cycle 10.1016/j.applthermaleng.2009.04.013 : Applied Thermal Engineering | ScienceDirect.com. Appl Therm Eng 2009;29:3094–102.

[34] Ibarra M, Rovira A, Alarcón-Padilla DC, Blanco J. Performance of a 5kWe Organic Rankine Cycle at part-load operation. Appl Energy 2014;120:147–58. doi:10.1016/j.apenergy.2014.01.057.

[35] Kane M, Larrain D, Favrat D, Allani Y. Small hybrid solar power system. Energy

2003;28:1427–43. doi:10.1016/S0360-5442(03)00127-0.

[36] Balje O. Turbomachines : a guide to design, selection and theory. John Wiley & Sons; 1981.

[37] Thome JR. Engineering data book III. Wolver Tube Inc 2004;2010.

[38] Peterson RB, Wang H, Herron T. Performance of a small-scale regenerative Rankine power cycle employing a scroll expander. Proc Inst Mech Eng Part A J Power Energy 2008;222:271–82. doi:10.1243/09576509JPE546.

[39] Lemort V, Quoilin S, Cuevas C, Lebrun J. Testing and modeling a scroll expander integrated into an Organic Rankine Cycle. Appl Therm Eng 2009;29:3094–102. doi:http://dx.doi.org/10.1016/j.applthermaleng.2009.04.013.

[40] Sanden USA n.d. http://www.sanden.com/aboutus.html (accessed February 14, 2017).

[41] Orosz MS, Mueller A V., Dechesne BJ, Hemond HF. Geometric Design of Scroll Expanders Optimized for Small Organic Rankine Cycles. J Eng Gas Turbines Power 2013;135:42303. doi:10.1115/1.4023112.

[42] Rosset K, Mounier V, Guenat E, Pajot O, Schiffmann J. Potential of Small-Scale Turbomachinery for Waste Heat Recovery on Automotive Internal Combustion Enginges. 3rd Int. Semin. ORC Power Syst., Brusse: 2015, p. 1–10.

[43] Bell IH, Lemort V, Groll EA, Braun JE, King GB, Horton WT. Liquid flooded compression and expansion in scroll machines - Part II: Experimental testing and model validation. Int J Refrig 2012;35:1890–900. doi:10.1016/j.ijrefrig.2012.07.008.

[44] Reed JR. Study of the feasibility and energy savings of producing and pre-cooling hydrogen with a 5kW ammonia based combined power coolling cycle 2004.

[45] Quoilin S, Lemort V, Lebrun J. Experimental study and modeling of an Organic Rankine Cycle using scroll expander. Appl Energy 2010;87:1260–8. doi:10.1016/j.apenergy.2009.06.026.

[46] Johnston JJR. Evaluation of expanders for use in a solar powered rankine cycle heat engine 2001.

[47] Ali Tarique M, Dincer I, Zamfirescu C. Experimental investigation of a scroll expander for an organic Rankine cycle. Int J Energy Res 2014;38:1825–34. doi:10.1002/er.3189.

[48] Baral S, Kim D, Yun E, Kim KC. Energy, exergy and performance analysis of small-scale organic rankine cycle systems for electrical power generation applicable in rural areas of developing countries. Energies 2015;8:684–713. doi:10.3390/en8020684.

[49] Morishita, Etsuo, Mutsuo Sekiya, and others. “A Co-Rotating Scroll Compressor for Positive Displacement and Centrifugal Dual-Mode Operations,” 1994. http://docs.lib.purdue.edu/cgi/viewcontent.cgi?article=2053&context=icec.

[50] Dutour, Sébastien, Hervé Carrier, Jean-Luc Daridon, Bernard Lagourette, and Guang-Hua Gao. 2002. “Speed of Sound, Density, and Compressibility of Alkylbenzenes as a Function of Pressure and Temperature: Tridecylbenzene and Pentadecylbenzene.” *Journal of Chemical & Engineering Data* 47 (6): 1532–36. https://doi.org/10.1021/je025560n.

[51] Sundaresan, Sonny G. 2015. “Compressor Lubrication -the Key to Performance.” *IOP Conference Series: Materials Science and Engineering* 90 (1): 012001. https://doi.org/10.1088/1757-899X/90/1/012001.

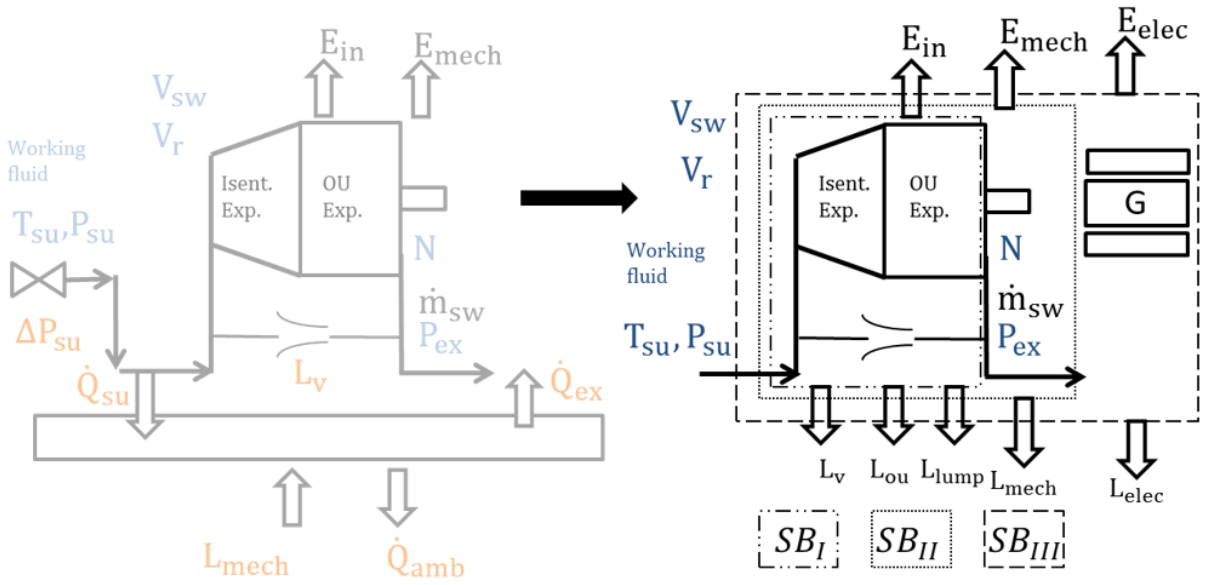

Figure 1 (a) Original 0D scroll expansion model. (b) Simplified model with extended system boundaries.

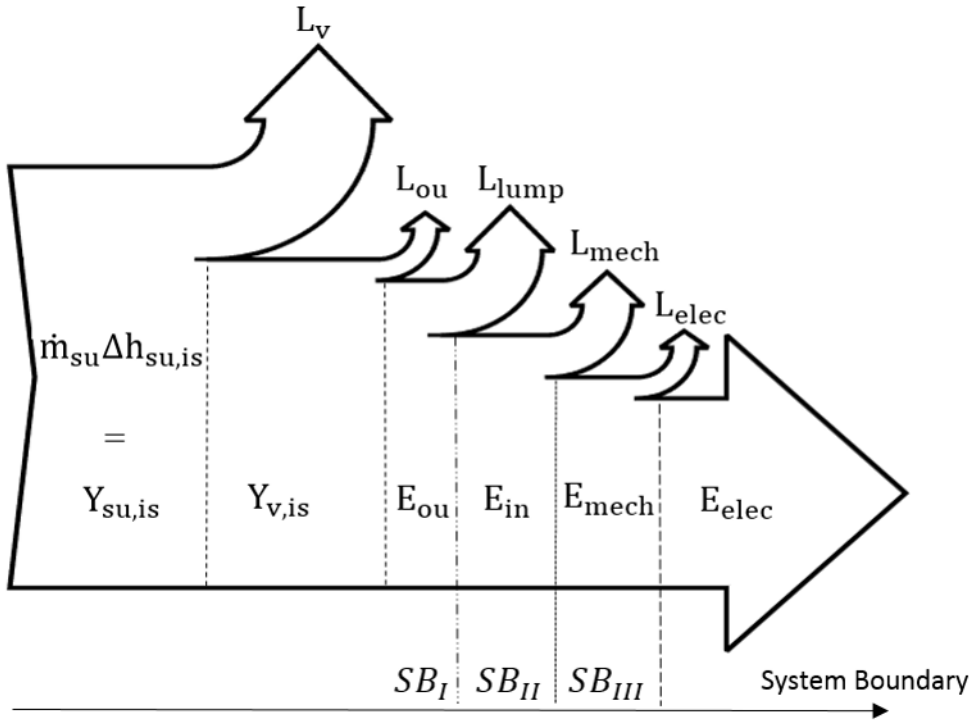

Figure 2 Scroll expander Sankey diagram for simplified scroll model of Figure 1 (b).

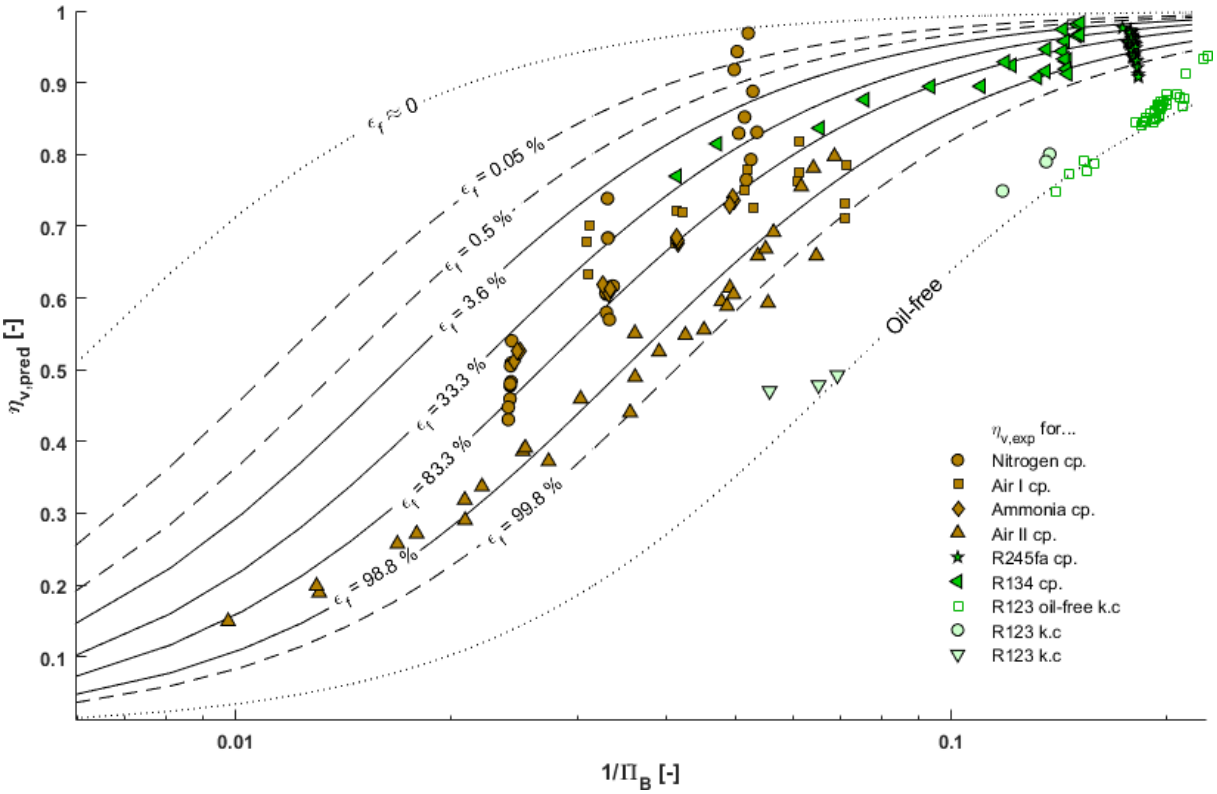

Figure 3 Volumetric efficiency based on Eq. 13 as a function of Π_B and of the void fraction ϵ_f (lines). Experimental scroll expander data out of literature is plotted for comparison (points) for the various working fluids, and scroll concepts (compliant and kinematically constrained).

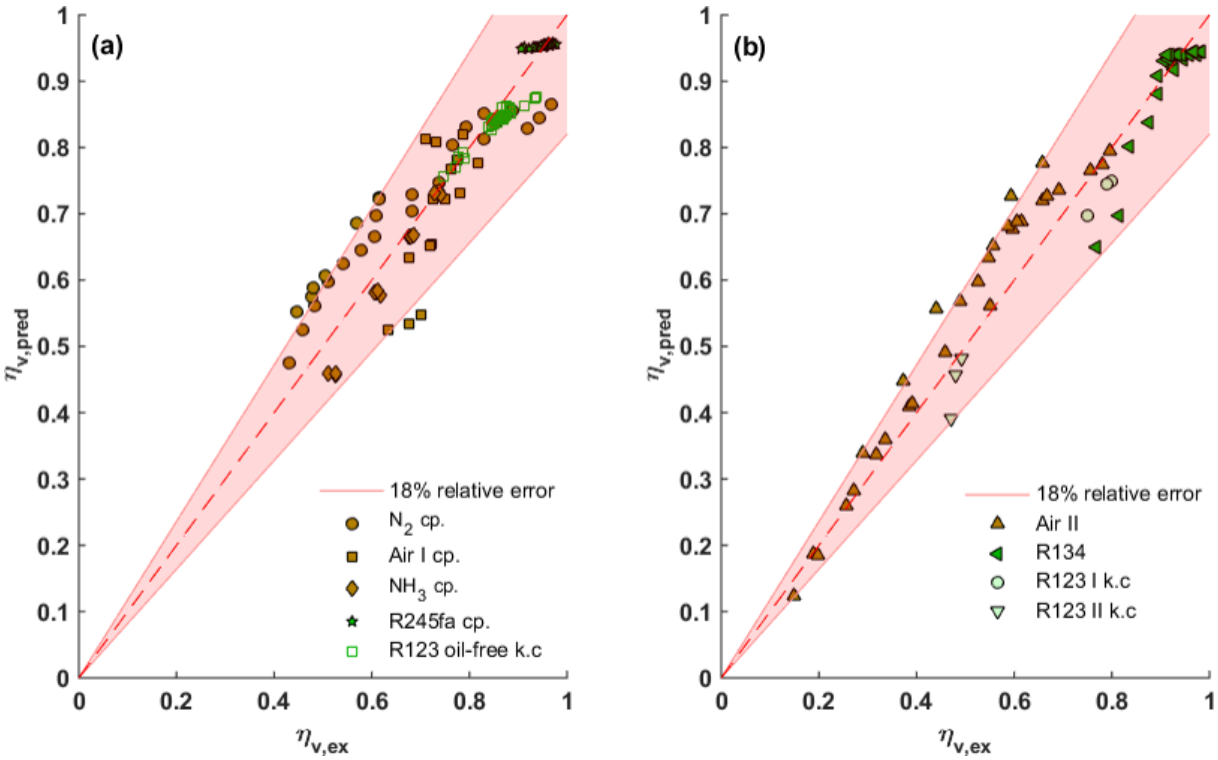

Figure 4 (a) Accuracy of calculated volumetric efficiency η_v (Eq. 13) against training data. (b) Accuracy of predicted η_v against experimental data not included in the training set. (But x_{oil} rough estimation based on Figure 3).

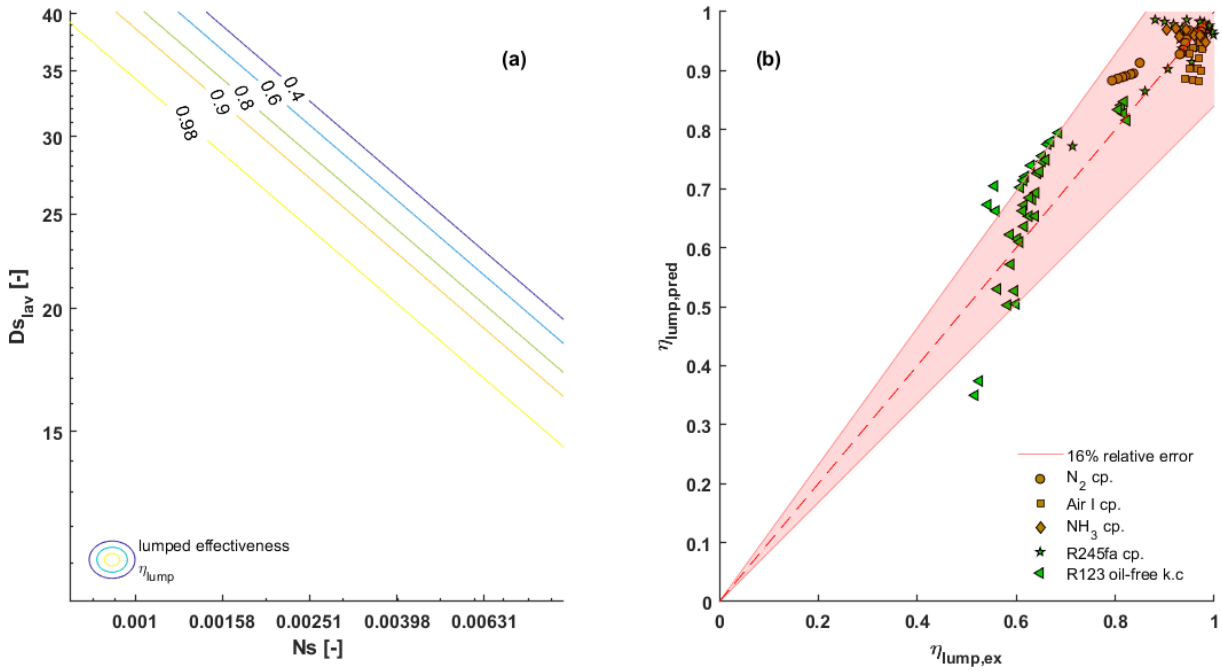

Figure 5 η_{lumped} based on the identified Eq. 18 and the comparison with experimental data as a function of specific speed Ns.

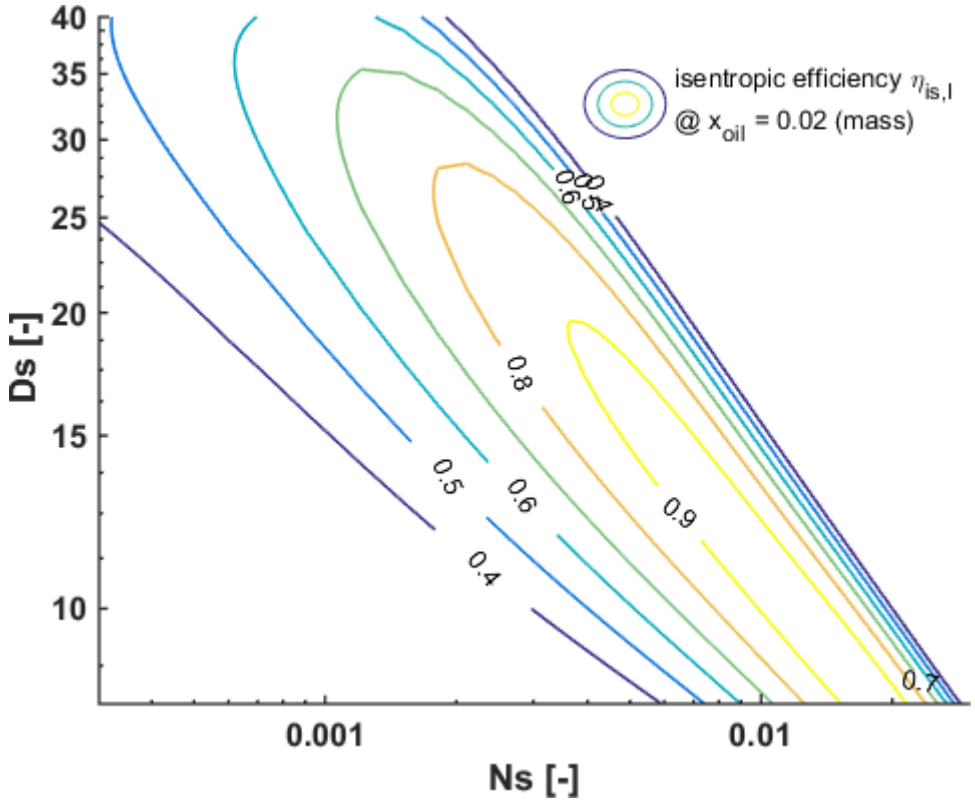

Figure 3 Scroll isentropic efficiency contours for adapted expansion as a function of Ns, Ds with normalized scroll diameter D* and oil mass fraction x_oil = 0.02.

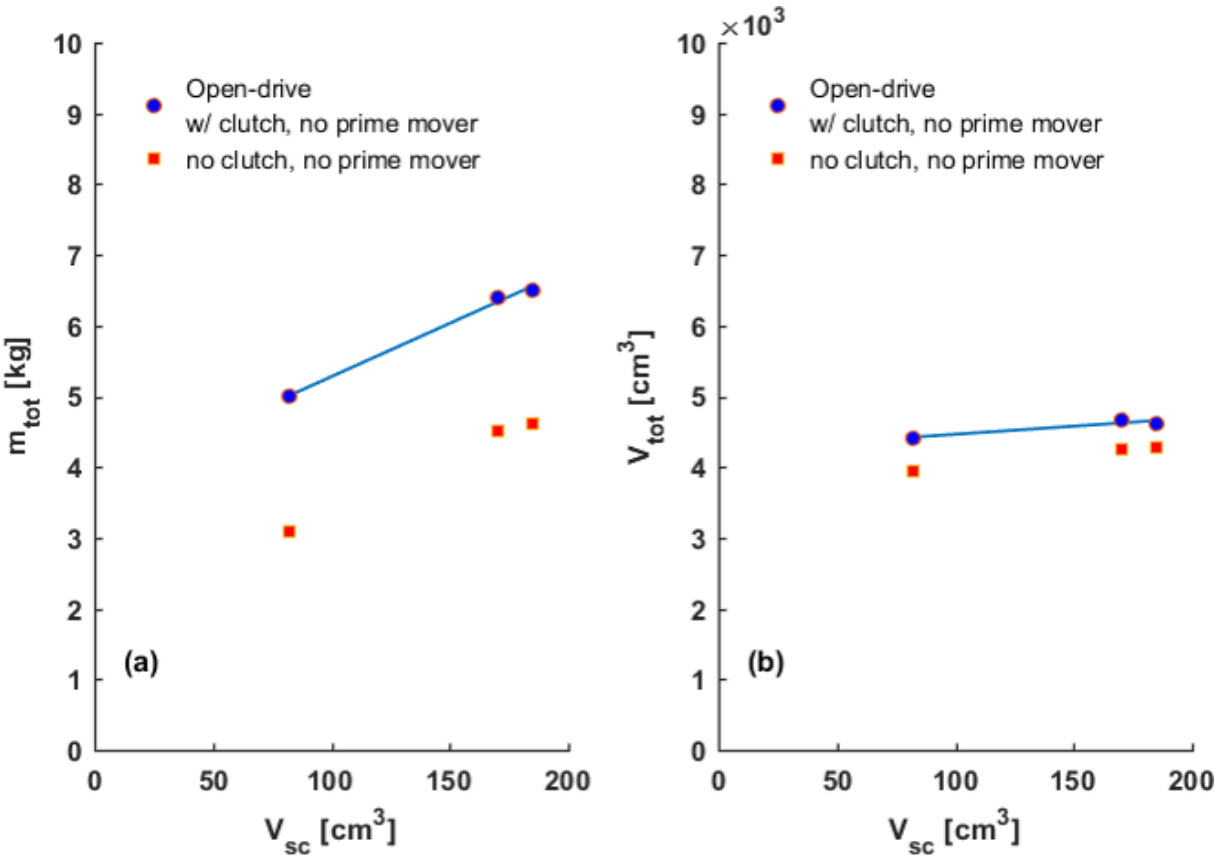

Figure 4 Open-drive scroll system total mass m_{tot} (a) and volume V_{tot} (b) as function of total scroll chamber volume V_{sc}.

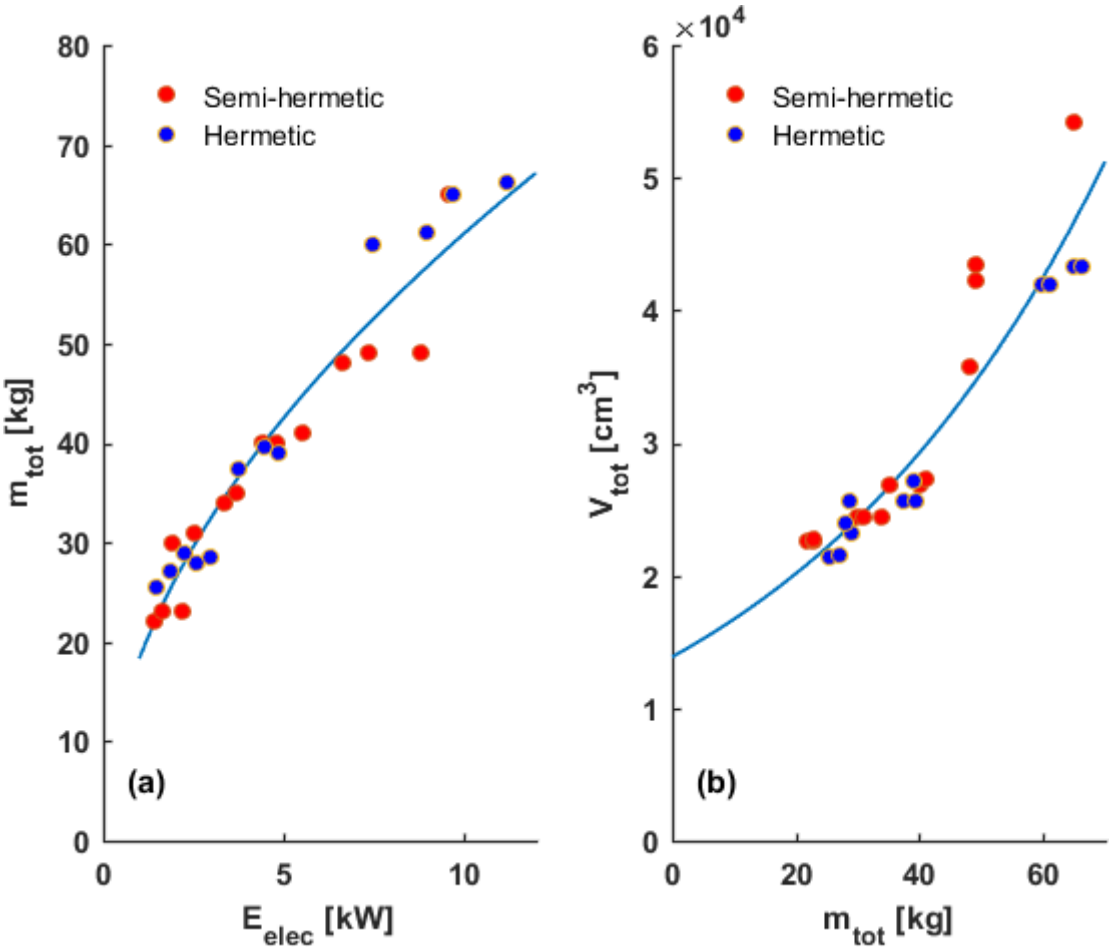

Figure 5 Direct-drive scroll system mass (a) and total volume (b) as a function of scroll total chamber volume according to manufacturer.

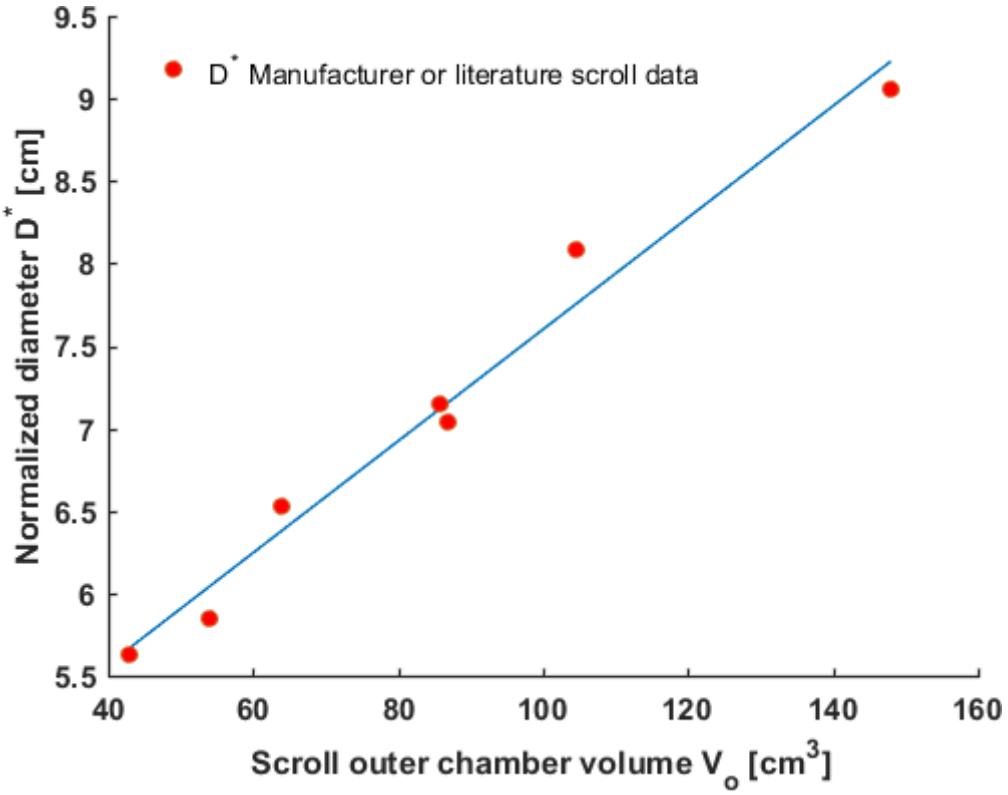

Figure 6 Normalized scroll diameter fit based on Eq. 22 as a function of scroll outer chamber volume Vo according to commercial compressors from Appendix A.

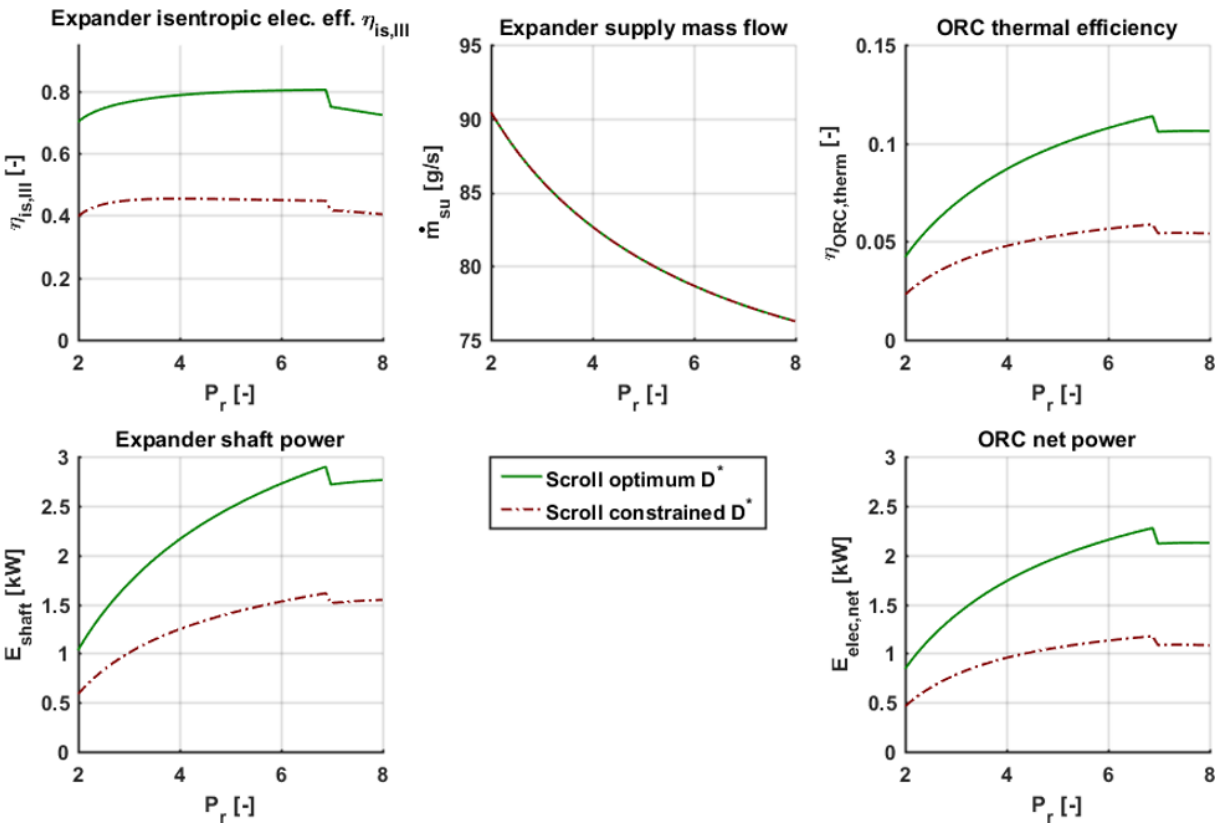

Figure 7 Performance indicators for ORC and scroll expanders for the waste heat recovery case study for passenger cars as a function of pressure ratio.

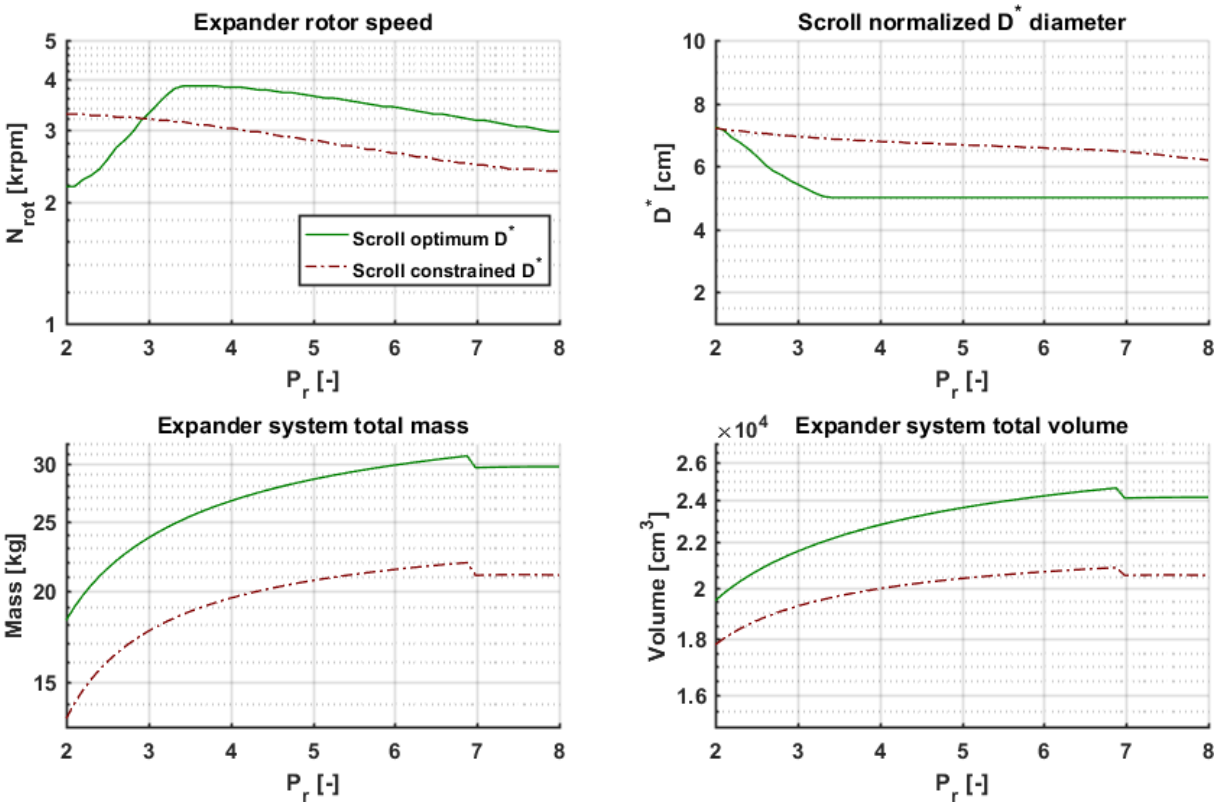

Figure 8 Scroll expander rotational speed and system sizing comparison under case study conditions as a function of pressure ratio.

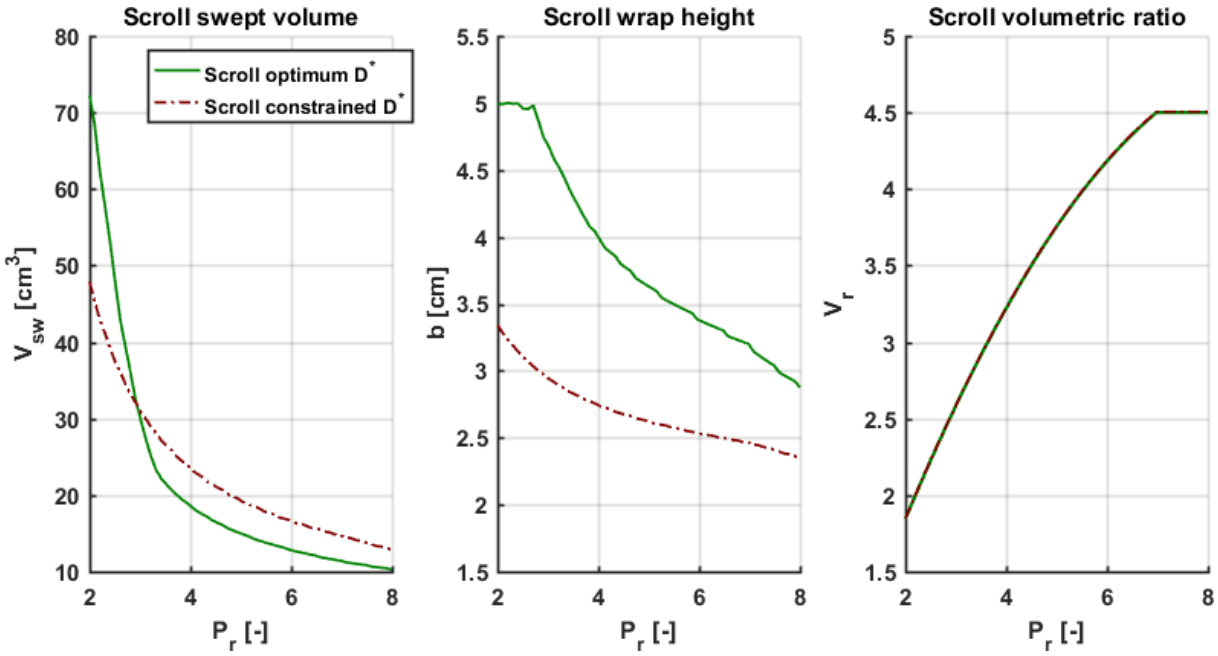

Figure 9 Scroll expanders best theoretical geometries under imposed operating conditions with varying pressure ratio.